Supporting Information

Nanoscale Control of Oxygen Defects and Metal-Insulator Transition in Epitaxial Vanadium Dioxides

*Yogesh Sharma[†], Janakiraman Balachandran[‡], Changhee Sohn[†], Jaron T. Krogel[†], Panchapakesan Ganesh[‡], Liam Collins[‡], Anton V. Ievlev[‡], Qian Li[‡], Xiang Gao[†], Nina Balke[‡], Olga S. Ovchinnikova[‡], Sergei V. Kalinin[‡], Olle Heinonen[§], Ho Nyung Lee[† *]*

[†]Materials Science and Technology Division, Oak Ridge National Laboratory, Oak Ridge, TN 37831, USA

[‡]Center for Nanophase Materials Sciences, Oak Ridge National Laboratory, Oak Ridge, TN 37831, USA

[§]Materials Science Division, Argonne National Laboratory, Lemont, IL 60439, USA

[*]hnlee@ornl.gov

This file includes;

The local I-V curves in CAFM measurements

We have measured the local current-voltage curves at low, high, and intermediate temperatures to compare the conductivity of the nanoscale clusters in the insulator to metal transition regime. The local I-V curves were acquired in the conductive AFM mode, applying bias to the conductive tip and measuring current through the sample. The local I-V curves from metallic and insulating domains at intermediate temperature (303 K) were compared with those obtained at high (330 K) and low (292 K) temperatures. To determine the I−V characteristics at different positions in the CAFM scan at 303 K (Fig. S2(b)), measurements were carried out at three separate points, as marked in Figure. The measurements were averaged over four separate sweeps. As expected from the CAFM scans, the I-V curves in Fig. S1(e), show three different conducting regions, point1 with high current (metallic), point2 with low current (insulating), and point3 with intermediate value of current.

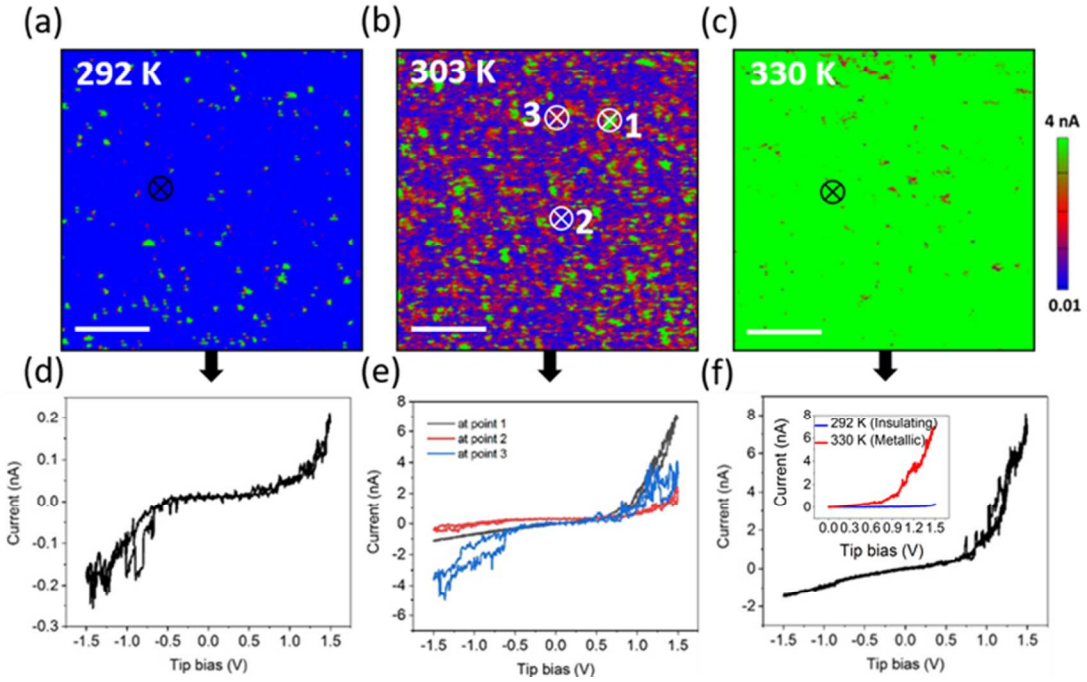

Figure S1. (a-c) CAFM maps and (d-f) local I-V curves measured at different temperatures. The I-V curves were measured in CAFM mode at the tip-positions marked in (a-c). Inset in Fig. (f) shows two order increase in current (read at 1.2 V) from 0.06 nA at 292 K in insulating phase to 3.87 nA at 330 K in metallic phase.

Concentric-square KPFM and CAFM measurements

In order to show reproducible modification or control of MIT under voltage bias from SPM tip in our VO_2 sample, concentric-square patterns were written by ± 4 V bias voltages at 298 K. CAFM and KPFM measurements were performed in them. As shown in Fig. S2 (a–b), the surface potential and current can indeed be well controlled by polarity-dependent tip-bias voltages. We switched the film surface into low resistance (metallic) state by applying negative bias voltages and then switched back into high resistance (insulating) state by positive bias voltage. This process was repeated two more times, switching high resistance state into low resistance state and then again low resistance to high resistance state, as shown in Fig. S2 (a). An AFM-topography image was also recorded after writing the patterns. We did not see any significant change in topography as evidenced in the line profile from the topography map in Fig. S2 (c). The line profiles from CAFM and KPFM maps [along red lines in (a) and (b)] further confirm the reproducible switching of surface potential and current in our VO_2 sample shown in Fig. S2 (d). The local I-V measurements were performed at 298 K, and bias was applied through the tip to the sample surface while grounding the bottom electrode (we were using a conducting Nb:STO substrate) through the current amplifier. Triangular unipolar pulses of the 1.5 V bias were used with simultaneous current acquisition from current amplifier. The measurements were averaged over four separate sweeps at each point marked in Fig. S2 (a). As expected from the CAFM scans, the I-V curves in Fig. S2(e) also showed two different conducting states; point-A

with lower current (insulating-VO_2), point-B with higher current (metallic-VO_2). The current values were found to be two orders of magnitude higher in the metallic areas compare to the insulating areas of the VO_2 film.

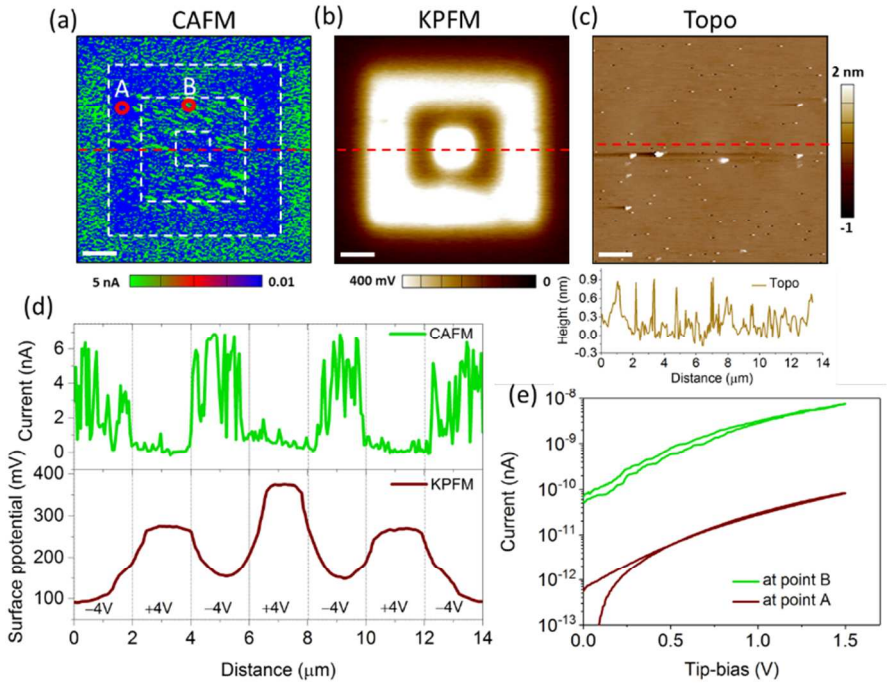

Figure S2. (a) CAFM, (b) KPFM, and (c) topography images of a VO_2 film after concentric-square patterning using tip-bias voltages of ± 4 V. (d) The line profiles from CAFM and KPFM images (a and b) along the red lines. (e) The I-V curves were recorded at two specific positions from those indicated in (a). The curves are consistent with the current contrast observed in (a).

Temperature dependent KPFM measurements

To gain more insight into the surface chemical potential change across the insulator to metal transition, we recorded KPFM images of the electrically written and pristine areas of the film while increasing the stage temperature from 278 to 348 K as shown in Fig. S3 (a). As represented in Fig. S3 (b), we observed that contact potential difference (CPD) between tip and sample decreases with increasing temperature. The lowering in CPD at higher temperatures near

the MIT can be explained by a decreased charge transfer gap due to the appearance of metallic nanodomains in the film as confirmed by CAFM measurements. However, we cannot neglect the charge relaxation processes caused by thermal effects at higher temperatures.

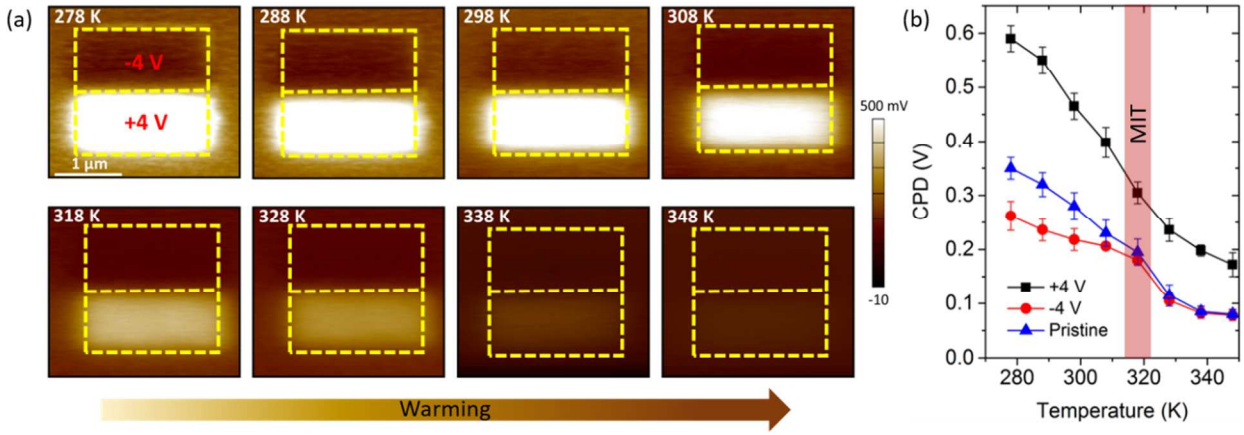

Figure S3. (a) Temperature dependent KPFM images of the electrical written areas. We observed reduced surface potential on the onset of insulator to metal transition. (b) The variation of CPD with temperature can be explained by thermal induced charge relaxation as well as decreased charge transfer gap due to appearance of metallic nanodomains in the film.

We have noticed that the values of CPD in the positive tip-bias written area are comparatively higher even if the film is in the metallic phase at higher temperatures, where the charge transfer gap is almost negligible and therefore the entire scan area should show nearly uniform surface potential. On the other hand, the temperature dependent change in CPD for the negative tip-bias written area is smaller than that in pristine and positive tip-bias written areas. Therefore, these results indicate that we can locally tune the oxygen stoichiometry in our VO_2 films via polarity control of the applied tip-bias voltage without chemical modification. In addition, we observed a sharp change (decrease) in the CPD value at the onset of the insulator to metal transition temperature as shown in the Fig. S3 (b). Such a sharp decrease in CPD can be

explained by the major contribution of structural phase transition leading to bulk metallization of the VO_2 film.

ToF-SIMS detection of H^+ ions

The hydrogenation could significantly affect the electrical conductivity of vanadium dioxide thin films, where surface moisture is one of the factors invoked to explain such biased tip-induced dissociation of water molecule at film surface. We have employed combined ToF-SIMS and AFM studies to investigate the role of the surface protonation or hydrogenation effect on enhanced electrical conductivity in negative biased area of VO_2 film. We have not observed any change in the concentration of H^+ ions, comparing with VO^+ ions, in pristine and electrically written areas (Fig. S4 (a) and (b)). The line profile (Fig. S4 (c)) along the dash line in Fig S4 (a) and (b), and the depth profile analysis (within the negative biased (-4V) written area), show that there is no change in the H^+ ions concentration on the surface and even in the bulk of the sample. These results indicate that hydrogenation cannot be a prominent factor for enhanced conductivity in our VO_2 films.

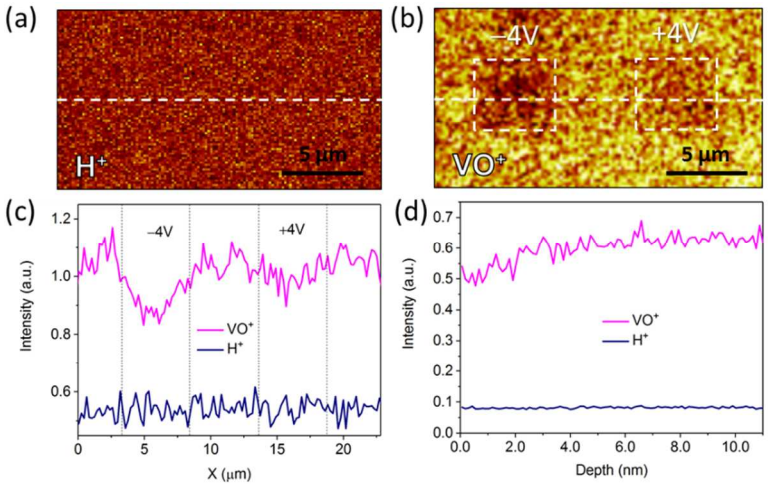

Figure S4. ToF-SIMS imaging of the sample surface including the regions electrically written by tip-bias voltages of –4 V (left) and +4 V (right): spatial distribution of (a) H^+ and (b) VO^+. (c)

The line profiles of the variation of H^+ and VO^+ ions concentration along the scan areas in (a) and (b), and (d) depth profile of the H^+ and VO^+ ions concentration within the –4 V electrically written regions.

Persistency of the electrically written patterns over time

We performed KPFM measurements on the patterned areas in different time intervals to observe the change in the surface chemical potential. Fig. S5 displays the KPFM images and the corresponding contact potential difference (CPD) line profiles of the written patterns in as-written state as well as after 6, and 11 hours, indicating the robustness of maintaining the oxygen concentration change induced by electrical writing. Since the changes in the CPD can be clearly seen even after 11 hours, we consider the electrically written area to last for a long period. However, despite kinetically slow, an oxygen backfilling will eventually happen as observed in a recent KPFM study on a STO thin film.[1]

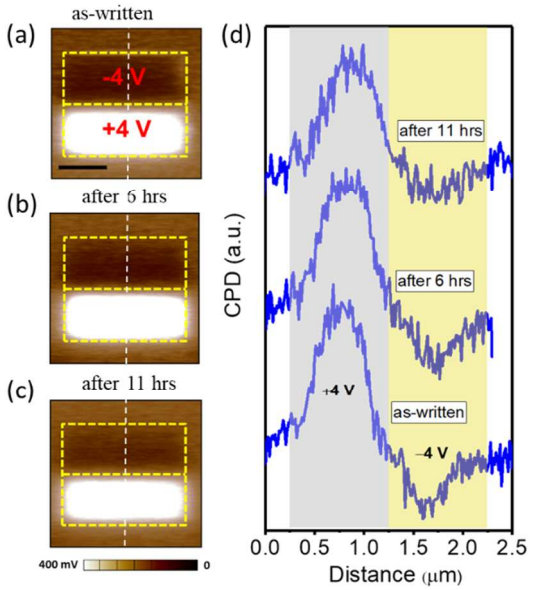

Figure S5 (a-c) KPFM measurements in different time intervals on the electrical written areas of the VO2 film. (d) Corresponding CPD profiles from KPFM images.

DFT+U calculations

Bulk studies of both the R and M1 phases of VO_2 in the literature[2-4]suggest the importance of incorporating orbital-dependent potentials in our DFT calculations. In addition to this, the gap-opening in the M1 phase in VO_2 is thought to be due to strong electron-electron correlations captured partly by range-separated hybrid functionals belonging to the HSE-family[5], which incorporate some amount of exact-exchange to the local- or semi-local exchange in regular DFT. But later studies show that HSE gives a poor description of the phase-stability as well as magnetism in bulk VO_2.[2] As such, in this study, we incorporate electronic correlations through a simple DFT+U scheme[6], using the PBE-flavor[7] of the exchange-correlation functional, as implemented in the plane-wave VASP package using PAW potentials[8,9]. This allows us to capture the effects of electron localization, resulting from correlation effects, while at the same time capturing to some extent the local orbital dependence of the full potential.

The value of 'U' in PBE+U calculations is not known *a priori*. To obtain a value for U in our study, we performed quantum Monte Carlo (QMC) calculations of the bulk M1 phase with the open source QMCPACK code.[10] QMC is the most accurate ground-state electronic structure method[11] for solids and it is also competitive with high level quantum chemistry methods for molecules. In particular, we employ the diffusion Monte Carlo (DMC) flavor of QMC methods, within the fixed-node approximation[12]. The total energy obtained from DMC is variational with respect to the parameters that enter the trial-wavefunction, which typically comes from a DFT calculation of the solid, and the true ground-state energy is obtain by minimizing this total-energy. By varying 'U', one can then generate a family of trial wavefunctions, and obtain the optimal value of 'U' (U_{opt}) which variationally minimizes the QMC total energy for the solid by optimizing the nodal surface of the many-body wavefunction. As shown in Fig. S6, the QMC

total energy shows a minimum at U_{opt}=4 eV, for trial wavefunctions generated with the PBE+U method.

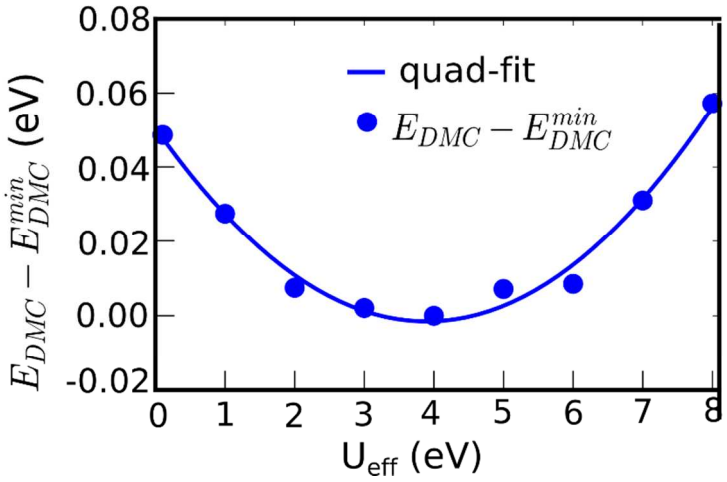

Figure S6. Ground state energy obtained for M1 phase employing QMC (diffusion Monte Carlo approach) as a function of effective parameter (U_{eff}).

We note that while obtaining an optimal U improves the quality of the ground-state electronic structure, it does not guarantee that we will also obtain an improved description of excited state orbitals (correct band-gap), though we do find a better agreement with experiments than the regular PBE-gaps.

References

1. Das, S.; Wang, B.; Cao, Y.; Cho, M. R.; Shin, Y. J.; Yang, S. M.; Wang, L.; Kim, M.; Kalinin, S. V.; Chen, L.Q.; Noh, T. W. Controlled Manipulation of Oxygen Vacancies Using Nanoscale Flexoelectricity. *Nat Commun.* **2017**, 8, 615.
2. Xiao, B.; Sun, J.; Ruzsinszky, A.; Perdew, J. P. Testing the Jacob's Ladder of Density Functionals for Electronic Structure and Magnetism of Rutile VO_2. *Phys. Rev. B* **2014**, 90, 085134.

3. Eyert, V. VO_2: A Novel View from Band Theory. *Phys. Rev. Lett.* **2011**, 107, 016401.
4. Zhu, Z.; Schwingenschlogl, U. Comprehensive Picture of VO_2 from Band Theory. *Phys. Rev. B* **2012**, 86, 075149.
5. Heyd, J.; Scuseria, G. E. Hybrid Functionals Based on A Screened Coulomb Potential. *The Journal of Chemical Physics* **2003**, 118, 8207.
6. Dudarev, S. L.; Botton, G. A.; Savrasov, S. Y.; Humphreys, C. J.; Sutton, A. P. Electron-Energy-Loss Spectra and the Structural Stability of Nickel Oxide: An LSDA+ U Study. *Phys. Rev. B* **1998**, 57, 1505.
7. Perdew, J. P.; Burke, K.; Ernzerhof, M. Generalized Gradient Approximation Made Simple. *Phys. Rev. Lett.* **1996**, 77, 3865.
8. Kresse, G.; Joubert, D. From Ultrasoft Pseudopotentials to the Projector Augmented-wave Method. *Phys. Rev. B* **1999**, 59, 1758.
9. Blöchl, P. E. Projector Augmented-wave Method. *Phys. Rev. B* **1994**, 50, 17953.
10. Kim, J.; Esler K. P.; McMinis, J.; Morales, M. A.; Clark, B. K.; Shulenburger, L.; Ceperley, D. M. Hybrid Algorithms in Quantum Monte Carlo. *J. Phys.: Conf. Ser.* **2012**, 402, 012008.
11. Foulkes, W. M. C.; Mitas, L.; Needs, R. J.; Rajagopal, G. Quantum Monte Carlo Simulations of Solids. *Rev. Mod. Phys.* **2001**, 73, 33.
12. Reynolds, P. J.; Ceperley, D. M.; Alder, B. J.; Lester, W. A. Fixed□node Quantum Monte Carlo for Molecules. *J. Chem. Phys.* **1982**, 77, 5593–5603.